Pulse Distortion on Multilayer Coupled Microstrip Lines

JAMES P. GILB, STUDENT MEMBER, IEEE, AND CONSTANTINE A. BALANIS, FELLOW, IEEE

Abstract—**The distortion of pulses due to dispersion and coupling on generalized planar microstrip is investigated. A simple, general form for the Green's function is obtained by solving the boundary value problem separately for the TE^y and TM^y modes. The mechanism of even/odd-mode distortion is discussed and numerical results are presented illustrating its effect. The design of structures with low even/odd-mode distortion is considered. Results for pulse distortion on this type of microstrip are also included.**

I. INTRODUCTION

ULTRAFAST switching speeds and decreasing circuit dimensions of MMIC's emphasize the dispersive nature of these printed circuit transmission lines. This increase in dispersive behavior can result in significant distortion on signals that travel only a short distance in an MMIC line. Signal distortion and the close proximity of additional transmission lines necessitate an accurate time-domain analysis of coupling between these lines. The distortion of nonperiodic signals on single microstrip lines has been investigated using approximate formulas for the line parameters [1]–[4], and experimental results have been published as well [4], [5]. Similar calculations have also been performed using approximate formulas to include the effects of attenuation distortion and a full-wave analysis to determine the effective dielectric constant [6], [7]. In addition, distortion effects on coplanar waveguides have been investigated [8]–[10], since their two-conductor structure makes the analysis almost the same as the single microstrip. Distortion of signals on multiple strips has also been examined using an impedance matrix approach with the matrix values determined from approximate formulas [11], [12]. However, a full-wave analysis of pulse distortion on multiple microstrip lines including the response on adjacent lines has not been investigated.

This paper uses a frequency-domain approach to analyze the time-domain response of a nonperiodic input in a multiconductor, multilayer microstrip structure. First the frequency-dependent propagation constants are found for the structure using a modified spectral-domain technique. These values are then used with the Fourier transform of the pulse to determine the frequency-domain output. This output is inverse Fourier-transformed to give the modal time-domain waveform. Finally, the modal waveforms are superimposed, giving the total response at a certain distance or time on all the conductors.

The propagation constants are found using a variation of the spectral-domain approach that is simple to formulate, computationally efficient, and easy to expand to examine very general structures. The derivation uses TE^y (LSE) and TM^y (LSM) modal configurations to expand the electric and magnetic fields. These configurations make the derivation much easier because the boundary value problem can be solved for each mode independently, streamlining the derivation and reducing the chance for errors. The resulting Green's function is purely real for lossless structures, thus reducing computer storage requirements and run times. Finally, the derivation can be applied to a very general geometry that includes all of the following:

a) an unlimited number of signal conductors confined to one plane;
b) an unlimited number of dielectric layers above and below the interface containing the conductors;
c) top (cover) and/or bottom (ground plane) conductor (either present or absent);
d) conductor sidewalls (either present or absent).

Results are presented showing that differences in the even- and odd-mode propagation constants can produce significant degradation of the pulse before it experiences degradation due to the dispersive nature of the structure. Graphs showing the effects of strip spacing on the shape of the signal pulse as well as the response on the sense line are included. It is also shown that the introduction of a substrate layer with a much lower dielectric constant and the proper height can cause the even- and odd-mode propagation constants to be equal, eliminating interference between the lines.

Manuscript received September 26, 1988; revised May 4, 1989. This work was supported by the U.S. Army Research Office under Contract DAAG29-85-K-0078.

The authors are with the Department of Electrical and Computer Engineering, Arizona State University, Tempe, AZ 85287.

IEEE Log Number 8929899.

0018-9480/89/1000-1620$01.00

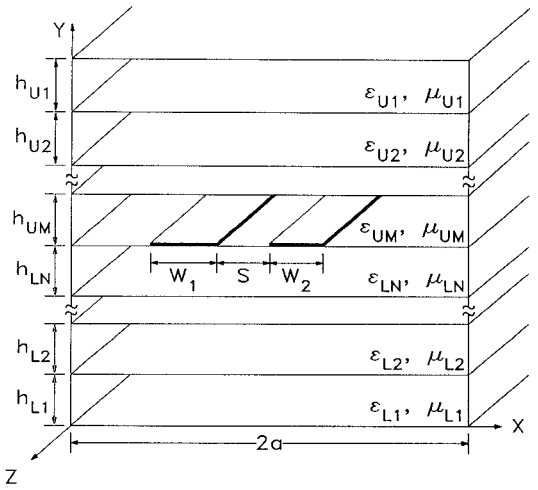

Fig. 1. Geometry of general planar coupled microstrip structure.

II. Dispersion Relations

Throughout the paper an $e^{j\omega t}$ time convention is used along with a two-dimensional spatial Fourier transform pair defined as

$$\mathcal{F}\{g(x,y,z)\} = \tilde{G}(\beta_x, y, \beta_z) = \int_{-\infty}^{\infty}\int_{-\infty}^{\infty} g(x,y,z)e^{j(\beta_x x+\beta_z z)}\,dx\,dz \quad (1)$$

$$\mathcal{F}^{-1}\{\tilde{G}(\beta_x, y, \beta_z)\} = g(x,y,z) = \frac{1}{(2\pi)^2}\int_{-\infty}^{\infty}\int_{-\infty}^{\infty} \tilde{G}(\beta_x, y, \beta_z)e^{-j(\beta_x x+\beta_z z)}\,d\beta_x\,d\beta_z \quad (2)$$

where $\beta_x^2+\beta_z^2-\alpha_y^2=\beta^2=\omega^2\mu\epsilon$, and β_x, β_z, and α_y are the wavenumbers in the x, z, and y directions. All Fourier transform quantities are denoted by a (~). The geometry used in the derivation of the Green's function for an arbitrary planar microstrip structure is shown in Fig. 1. The structure is surrounded on four sides by perfect electric conductors at $x=\pm a$, $y=0$, and $y=h_{L1}+h_{L2}+\cdots+h_{U2}+h_{U1}$. If an open structure is to be considered, then $a\to\infty$ and $h_{U1}\to\infty$. For a covered microstrip without sidewalls, then $a\to\infty$ with h_{U1} remaining finite.

The propagation constant $\beta_z(\omega)$ can be determined in many ways. However for coupled microstrips, the spectral-domain approach is simple to formulate and apply, and it can be easily extended to many different structures. This paper uses a variation of the spectral-domain approach to derive the Green's function of the microstrip. This variation is computationally efficient because the Green's function is expressed as a real function over the entire range of integration. In addition, the formulation shows that the boundary conditions can be enforced on the TE^y and TM^y modes independently. This allows the total boundary value problem to be split into two smaller, similar problems, greatly reducing the complexity of the derivation.

In order to show that a TE or a TM mode can be used independently to solve the boundary value problem, it is necessary to demonstrate that the tangential field components satisfy all the boundary conditions over a closed surface, with no conflicting conditions. This condition is valid for the TE^y and TM^y modes, in contrast to the TE^z and TM^z modes, if certain conditions on the modal current densities are met [13]. In particular, the x and z modal current densities must be related by

$$\beta_z\tilde{J}_z^{\mathrm{TE}} = -\beta_x\tilde{J}_x^{\mathrm{TE}} \quad (3a)$$

$$\beta_x\tilde{J}_z^{\mathrm{TM}} = \beta_z\tilde{J}_x^{\mathrm{TM}}. \quad (3b)$$

The first equation is derived by using the continuity equation in the transform domain and the second by using the magnetic wave equation in the transform domain [13]. In addition, the modal currents are related to the total current density on the microstrip by

$$\tilde{J}_z = \tilde{J}_z^{\mathrm{TM}} + \tilde{J}_z^{\mathrm{TE}} \quad (4a)$$

$$\tilde{J}_x = \tilde{J}_x^{\mathrm{TM}} + \tilde{J}_x^{\mathrm{TE}}. \quad (4b)$$

Thus, the modal current densities can be expressed in terms of the total current densities using (3a) and (3b) as

$$\tilde{J}_z^{\mathrm{TM}} = \frac{\beta_z(\tilde{J}_z\beta_z + \tilde{J}_x\beta_x)}{(\beta_x^2+\beta_z^2)} \quad (5a)$$

$$\tilde{J}_z^{\mathrm{TE}} = \frac{\beta_x(\tilde{J}_z\beta_x - \tilde{J}_x\beta_z)}{(\beta_x^2+\beta_z^2)}. \quad (5b)$$

Using these current densities, the total fields at the dielectric interface containing the center conductors can be written as

$$\tilde{E}_z = \frac{j}{\omega\epsilon_0}\left[\tilde{J}_z\tilde{G}_{zz} + \tilde{J}_x\tilde{G}_{xz}\right] \quad (6a)$$

$$\tilde{E}_x = \frac{j}{\omega\epsilon_0}\left[\tilde{J}_z\tilde{G}_{zx} + \tilde{J}_x\tilde{G}_{xx}\right] \quad (6b)$$

where $\tilde{G}_{xx}, \tilde{G}_{zx}$, and $\tilde{G}_{zz}$ are the dyadic Green's functions for the particular geometry being considered and are defined as

$$\tilde{G}_{zz} = \frac{\beta_z^2\tilde{Z}^{\mathrm{TM}} - \beta_x^2\beta_0^2\tilde{Z}^{\mathrm{TE}}}{\beta_x^2+\beta_z^2} \quad (7a)$$

$$\tilde{G}_{xx} = \frac{\beta_x^2\tilde{Z}^{\mathrm{TM}} - \beta_z^2\beta_0^2\tilde{Z}^{\mathrm{TE}}}{\beta_x^2+\beta_z^2} \quad (7b)$$

$$\tilde{G}_{xz} = \tilde{G}_{zx} = \beta_x\beta_z\frac{\tilde{Z}^{\mathrm{TM}} + \beta_0^2\tilde{Z}^{\mathrm{TE}}}{\beta_x^2+\beta_z^2} \quad (7c)$$

and $\tilde{Z}^{\mathrm{TE}}$ and $\tilde{Z}^{\mathrm{TM}}$ are the modal Green's impedance functions for the particular geometry being examined. A general recurrence relation to determine $\tilde{Z}^{\mathrm{TE}}$ and $\tilde{Z}^{\mathrm{TM}}$ for any arbitrary planar structure is presented in Section III. Equations (6a) and (6b) can then be solved for β_z via Galerkin's method as in [14].

III. Green's Function

While the Green's function for any arbitrary planar microstrip geometry can be derived using Maxwell's equations and enforcing the boundary conditions at the interfaces, the derivation becomes complex and tedious as more dielectric layers are considered. However there is a definite form that the Green's function takes as more planar dielectric layers are added. This form becomes apparent as the boundary value problem is solved for more than two dielectric layers above or below the conductor interface. The impedance elements of the Green's function, $\tilde{Z}^{\mathrm{TM}}$ and $\tilde{Z}^{\mathrm{TE}}$, can be written as a parallel combination of the admittances seen above and below the conductor interface; i.e,

$$\tilde{Z}^{(i)} = \frac{1}{\tilde{Y}^{(i)}_{LN} + \tilde{Y}^{(i)}_{UM}} \tag{8}$$

where i is either TE or TM; L and U indicate the lower and upper layers respectively; and N and M are the total numbers of planar layers below and above the interface, as in Fig. 1.

The admittances $\tilde{Y}^{(i)}_{(j)}$ can be found using a recursive formulation for either the upper or the lower layer, beginning with $j = L1$ or $U1$ through $j = LN$ or UM, using

$$\tilde{Y}^{\mathrm{TM}}_{(j)} = \frac{\tilde{Y}^{\mathrm{TM}}_{s(j)}\tilde{Y}^{\mathrm{TM}}_{(j-1)} + \alpha^2_{y(j)}/\mu_{r(j)}}{\tilde{Y}^{\mathrm{TM}}_{s(j)} + \tilde{Y}^{\mathrm{TM}}_{(j-1)}} \tag{9a}$$

$$\tilde{Y}^{\mathrm{TE}}_{(j)} = \frac{\tilde{Y}^{\mathrm{TE}}_{s(j)}\tilde{Y}^{\mathrm{TE}}_{(j-1)} + \epsilon^2_{r(j)}/\alpha^2_{y(j)}}{\tilde{Y}^{\mathrm{TE}}_{s(j)} + \tilde{Y}^{\mathrm{TE}}_{(j-1)}} \tag{9b}$$

$$\tilde{Y}^{\mathrm{TE}}_{s(j)} = \frac{\alpha_{y(j)}\coth\left[\alpha_{y(j)}h_{(j)}\right]}{\mu_{r(j)}} \tag{9c}$$

$$\tilde{Y}^{\mathrm{TM}}_{s(j)} = \frac{\epsilon_{r(j)}\coth\left[\alpha_{y(j)}h_{(j)}\right]}{\alpha_{y(j)}}. \tag{9d}$$

$\tilde{Y}^{(i)}_{(j)}$ can be thought of as the admittance seen looking outward from the jth layer (away from the conductor interface), and $\tilde{Y}^{(i)}_{s(j)}$ is the self-admittance of the layer for the particular mode configuration.

For $j = U1$ or $L1$, then the $(j-1)$th layer, $U0$ or $L0$, is a perfect electric conductor (i.e., a ground plane or cover sheet), and $\tilde{Y}^{(i)}_{(k)0} \to \infty$, for $k = U$ or L, since a perfect conductor has zero resistance. Taking the limit of either (12a) or (12b) as $\tilde{Y}^{(i)}_{(k)0}$ goes to infinity leads to $\tilde{Y}^{(i)}_{(k)1} = \tilde{Y}^{(i)}_{s(k)1}$.

If the $(k)1$th layer is dielectric of infinite height (i.e., a structure with no ground plane or cover sheet), then $h_{(k)1} \to \infty$ and $\coth(\alpha_{y(k)1}h_{(k)1}) \to 1$. The conditions for $\tilde{Y}^{(i)}_{(k)0}$ and $\tilde{Y}^{(i)}_{(k)1}$ are the same as above, as though there were a conductor at an infinite distance. This is a valid assumption since the outward radiation condition specifies that $\boldsymbol{E} \to 0$ as $y \to \pm\infty$. This particular configuration, with no ground plane and/or cover sheet, results in

$$\tilde{Y}^{\mathrm{TE}}_{(k)1} = \tilde{Y}^{\mathrm{TE}}_{s(k)1} = \alpha_{y(k)1}/\mu_{r(k)1} \tag{10a}$$

$$\tilde{Y}^{\mathrm{TM}}_{(k)1} = \tilde{Y}^{\mathrm{TM}}_{s(k)1} = \epsilon_{r(k)1}/\alpha_{y(k)1}, \qquad k = U \text{ or } L. \tag{10b}$$

Note that these equations are the same for layers above and below the conductor interface because Maxwell's equations are invariant with respect to choice of coordinates. This is valid only for strips of vanishingly small thickness and becomes invalid when the strip thickness approaches the height of the dielectric layer that contains it.

IV. Pulse Dispersion

The voltage or electric field on the microstrip at any position z and time t_0 can be represented as

$$v(t_0, z) = \frac{1}{2\pi}\int_{-\infty}^{\infty} \tilde{V}(\omega, z=0)\, e^{j[\omega t_0 - \beta_z(\omega) z]}\, d\omega \tag{11}$$

where

$$\tilde{V}(\omega, z=0) = \int_{-\infty}^{\infty} v(t, z=0)\, e^{-j\omega t}\, dt \tag{12}$$

where $v(t, z=0)$ and $\tilde{V}(w, z=0)$ are a Fourier transform pair and $\beta_z(\omega)$ is the frequency-dependent z-directed propagation constant. In the case of a finite time-domain signal, the limits of the second integration are modified to include only the time that the pulse exists. This integration can often be done explicitly since many of the signals of interest have transforms that can be expressed in closed form.

Since the microstrip is a linear device with respect to time, the principle of superposition can be applied to the input signal so that it can be split into two simpler problems. For symmetric strips, the input signal is split into even- and odd-mode configurations. For the even mode, two in-phase signals whose amplitudes are one half of the original signal are propagated in both strips. This is equivalent to having a magnetic wall between the two strips. The odd mode has two signals of one half amplitude, but these signals are 180° out of phase. This is equivalent to having an electric wall separating the two strips. The effective dielectric constant for each of these modes can be easily calculated using the spectral-domain approach as outlined in Section II.

Having determined the time-dependent response of symmetric strips for each of the two modes, even and odd, the response to a single signal in line 1 and no excitation for line 2 is

$$v_1(t_0, z) = \frac{1}{2}\left[v_e(t_0, z) + v_o(t_0, z)\right] \tag{13a}$$

$$v_2(t_0, z) = \frac{1}{2}\left[v_e(t_0, z) - v_o(t_0, z)\right] \tag{13b}$$

where $v_e(t_0, z)$ and $v_o(t_0, z)$ are the even- and odd-mode responses of line 1 to the input signal. Also $v_1(t_0, z)$ and $v_2(t_0, z)$ are the voltages on lines 1 and 2 at time t_0 and position z. Using (11), the even- and odd-mode responses

can be written as

$$v_e(t_0, z) = \frac{1}{2\pi}\int_{-\infty}^{\infty} \tilde{V}(\omega, z=0)\, e^{j\omega[t_0 - z/c\sqrt{\epsilon_{re}}]}\, d\omega \quad (14a)$$

$$v_o(t_0, z) = \frac{1}{2\pi}\int_{-\infty}^{\infty} \tilde{V}(\omega, z=0)\, e^{j\omega[t_0 - z/c\sqrt{\epsilon_{ro}}]}\, d\omega \quad (14b)$$

where ϵ_{re} and ϵ_{ro} are the frequency-dependent effective dielectric constants for the even and odd modes, respectively, and c is the speed of light in free space. Substituting these two equations back into (13a) and (13b) and simplifying we can write

$$v_1 = \frac{1}{2\pi}\int_{-\infty}^{\infty} \tilde{V}\cos\left\{\omega\frac{z}{c}\frac{\sqrt{\epsilon_{re}} - \sqrt{\epsilon_{ro}}}{2}\right\} \cdot\exp\left\{j\omega\left[t_0 - \frac{z}{c}\frac{\sqrt{\epsilon_{re}} + \sqrt{\epsilon_{ro}}}{2}\right]\right\} d\omega \quad (15a)$$

$$v_2 = \frac{1}{2\pi}\int_{-\infty}^{\infty} j\tilde{V}\sin\left\{\omega\frac{z}{c}\frac{\sqrt{\epsilon_{re}} - \sqrt{\epsilon_{ro}}}{2}\right\} \cdot\exp\left\{j\omega\left[t_0 - \frac{z}{c}\frac{\sqrt{\epsilon_{re}} + \sqrt{\epsilon_{ro}}}{2}\right]\right\} d\omega. \quad (15b)$$

Since only the real part of the signal is of interest, the integrations can be written more simply as

$$v_1 = \frac{1}{2\pi}\int_{-\infty}^{\infty} \tilde{V}\cos\left\{\omega\frac{z}{c}\frac{\sqrt{\epsilon_{re}} - \sqrt{\epsilon_{ro}}}{2}\right\} \cdot\cos\left\{\omega t_0 - \omega\frac{z}{c}\frac{\sqrt{\epsilon_{re}} + \sqrt{\epsilon_{ro}}}{2}\right\} d\omega \quad (16a)$$

$$v_2 = -\frac{1}{2\pi}\int_{-\infty}^{\infty} \tilde{V}\sin\left\{\omega\frac{z}{c}\frac{\sqrt{\epsilon_{re}} - \sqrt{\epsilon_{ro}}}{2}\right\} \cdot\sin\left\{\omega t_0 - \omega\frac{z}{c}\frac{\sqrt{\epsilon_{re}} + \sqrt{\epsilon_{ro}}}{2}\right\} d\omega. \quad (16b)$$

V. Results

On lossless coupled microstrip lines, there are two mechanisms that degrade the signal: dispersion and coupling. Dispersion is due to the frequency-dependent behavior of ϵ_{reff}, causing the different frequency components of the pulse to travel at different speeds. Coupling, on the other hand, arises from a difference in the even- and odd-mode ϵ_{reff}. Both dispersion and coupling reduce the amplitude of the signal and spread it out in time. In addition, coupling has another important effect on signal transmission; it creates responses on adjacent lines.

Coupling distortion can best be understood by considering the response on both lines to be a linear combination of four pulses, two on each line, as in Fig. 2(a). In general, the in-phase pair (even) and the out-of-phase pair (odd) will travel down the line at two different speeds, due to differences in the ϵ_{reff} of the even and odd modes. The even- and odd-mode pairs of pulses add constructively on the signal line, and destructively on the sense line. To isolate the effects of even/odd-mode distortion, a hypothetical lossless and dispersionless two-conductor transmission line is considered. A rectangular pulse is used for simplicity, and it is assumed that the odd-mode ϵ_{reff} is higher than the even mode. When the signal first starts out, the even and odd pairs have not separated very much, and almost completely cancel each other on the sense line and reproduce the signal fairly accurately on the signal line, as shown in Fig. 2(b). As the signal travels farther (Fig. 2(c)), the even and odd pairs begin to separate. Now they do not cancel completely on the sense line or reproduce the signal very well on the signal line, the result being distortion and cross talk. After the signal travels a very great distance (Fig. 2(d)) the even- and odd-mode pairs separate completely. In Fig. 2(b)–(d), the leading response on the sense line is positive, because it was assumed that the even-mode ϵ_{reff} was less than the odd mode; if this is not the case, then the leading response is negative. In addition, as the distance increases, the amplitude of the response on both lines will tend to approach one half the value of the response on a single, isolated line. The total pulse spread, in time, due to even/odd distortion, at a distance z_0, can be written as

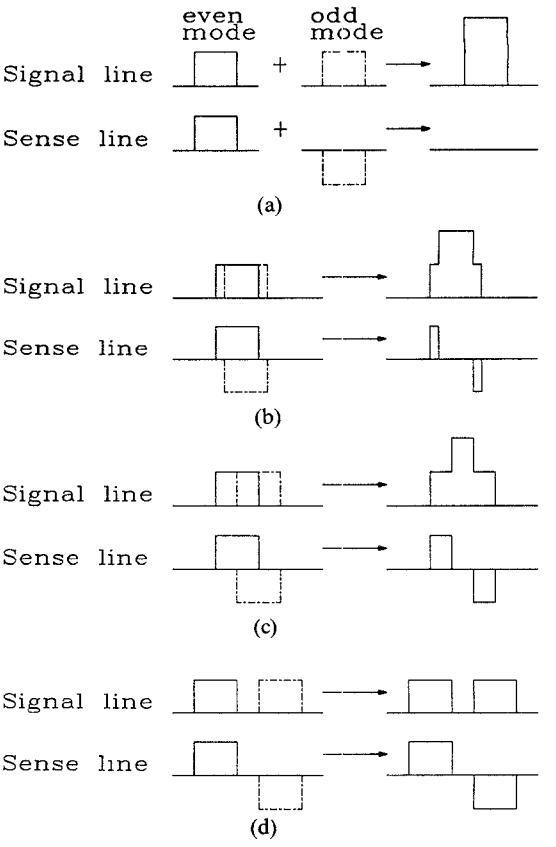

Fig. 2. Even/odd-mode disortion on a nondispersive, lossless transmission line. (a) Split into even and odd modes. (b) Distortion after a short distance. (c) Increasing distortion with distance. (d) Even and odd separate completely.

$$t_s = \frac{z_0}{c}\left[\sqrt{\epsilon_{re}} - \sqrt{\epsilon_{ro}}\right] \quad (17)$$

where ϵ_{re} and ϵ_{ro} are the ϵ_{reff} for the even and the odd

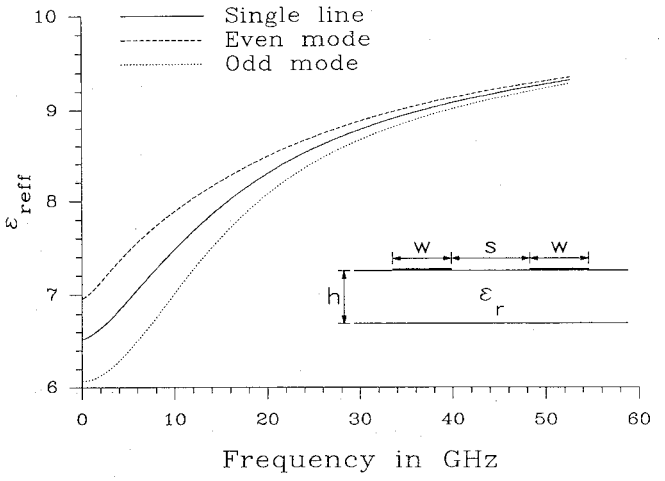

Fig. 3. Effective dielectric constants of a coupled microstrip and a single isolated microstrip ($w = h = 1.5$ mm, $s = 3.0$ mm, $\epsilon_r = 9.7$).

mode, respectively. If the transmission line is dispersive, then the even/odd distortion mechanism is the same, except that the even- and odd-mode pairs suffer dispersion as they travel down the line, adding additional pulse spread and further reducing the amplitude of the signal.

To illustrate these two mechanisms, Gaussian pulses are used, whose time and frequency responses are defined as

$$v(t) = Ae^{-\ln(2)(t/\tau)^2} \leftrightarrow \tilde{V}(\omega) = A\tau\sqrt{\frac{\pi}{\ln(2)}}\, e^{-(\omega\tau/2)^2/\ln(2)}. \tag{18}$$

Here A is the amplitude of the pulse, τ is the half maximum, half width time, and the pulse is centered about $t = 0$. For the computation of ϵ_{reff}, a 2 by 2 matrix is used ($M = N = 1$) with the $\tilde{J}_x$ from [14] and $\tilde{J}_z$ from [15]. Results obtained with this method have been compared and agree very closely with results presented in the literature [14], [16].

Fig. 3 shows ϵ_{reff} as a function of frequency for a single-layer symmetric coupled microstrip, whose dimensions are given in the figure. The change in ϵ_{reff} versus frequency is responsible for dispersion distortion while the differences in ϵ_{re} and ϵ_{ro} at a given frequency are responsible for coupling distortion. At higher frequencies, ϵ_{re} and ϵ_{ro} approach the same limiting value, ϵ_r; hence coupling distortion is less significant at these frequencies. The lines have greater isolation at the higher frequencies because the electrical distance between the lines becomes greater as the frequency increases. The largest differences between ϵ_{re} and ϵ_{ro} appear at low frequencies for this structure. Thus while a low-frequency-content pulse (i.e., long time duration and/or long rise times) would experience little dispersion distortion, due to the relatively constant ϵ_{reff} at low frequencies, it would still be very susceptible to coupling dispersion, due to the large difference in ϵ_{re} and ϵ_{ro} at the lower frequencies.

In order to illustrate the effects of dispersion and coupling distortion in the structure detailed in Fig. 3, a

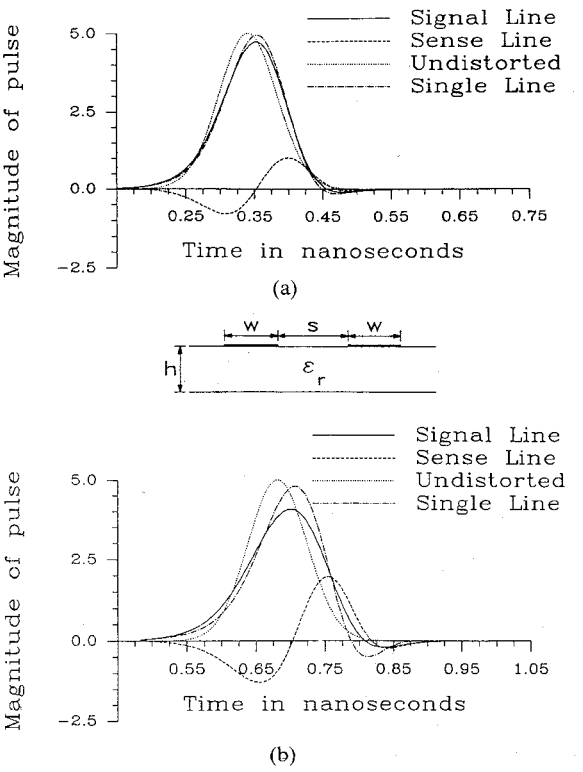

Fig. 4. Gaussian pulse distortion on a coupled microstrip and single isolated microstrip for (a) $l = 40$ mm and (b) $l = 80$ mm ($\tau = 50$ ps, $A = 5$, $w = h = 1.5$ mm, $s = 3.0$ mm, $\epsilon_r = 9.7$).

Gaussian pulse ($A = 5$, $\tau = 50$ ps) is assumed to enter the signal line, with no signal on the sense line. The response on both lines is plotted as a function of time in Figs. 4 and 5 at four different distances. For comparison, the response on a single isolated line on the same structure and an undistorted pulse are included. The undistorted pulse is computed using a constant ϵ_{reff} equal to its zero-frequency value for the single line. The difference between the pulses in the single and in the undistorted lines shows the effect of dispersion. The difference between the pulses in the single and the signal lines illustrates how coupling affects the transmitted pulse. In addition, the amount of cross talk is represented by the response on the sense line.

After the signal has traveled only a short distance, the even/odd-mode distortion begins to significantly affect the pulse. At 80 mm dispersion has reduced the pulse amplitude by only 4 percent, while even/odd distortion accounts for an extra 14 percent reduction. The response on the sense line has risen to almost 40 percent of the undistorted pulse height. By 160 mm, dispersion accounts for a 12 percent reduction while even/odd distortion accounts for an extra 30 percent, reducing the signal amplitude to almost half the original value. The response on the sense line has risen to 56 percent, achieving almost the same amplitude as the signal line response. At this distance, distortion due to dispersion is still not a major factor, while even/odd-mode distortion has critically degraded the pulse and induced a false signal on the sense line. Thus even/odd-mode distortion is the dominant mechanism for this structure.

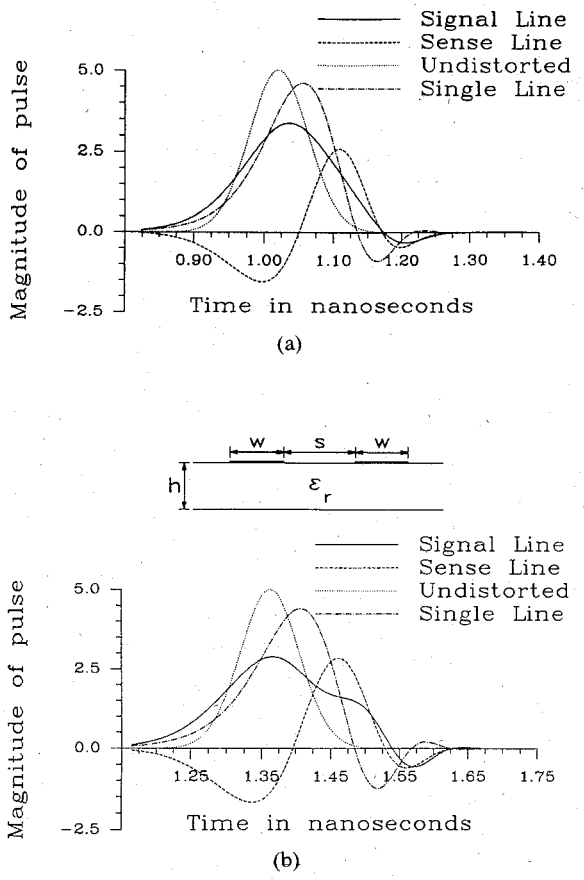

Fig. 5. Gaussian pulse distortion on a coupled microstrip and single isolated microstrip for (a) $l = 120$ mm and (b) $l = 160$ mm ($\tau = 50$ ps, $A = 5$, $w = h = 1.5$ mm, $s = 3.0$ mm, $\epsilon_r = 9.7$).

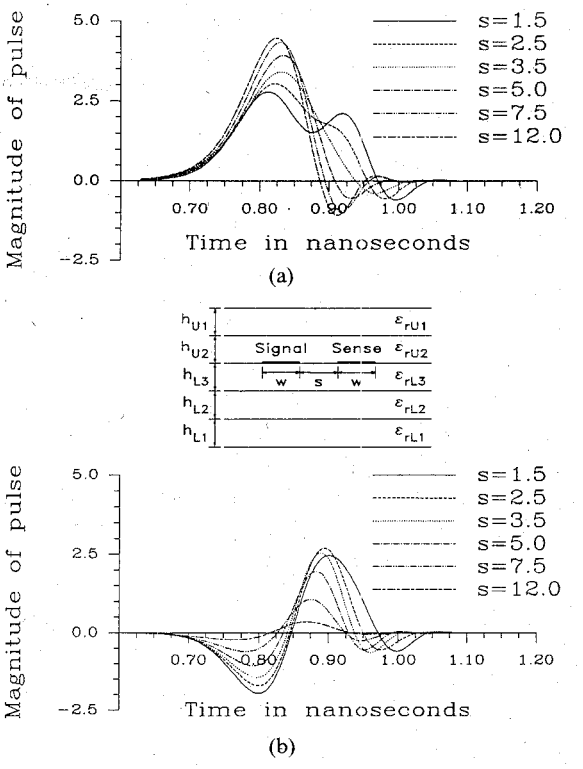

Fig. 6. Distortion of a Gaussian pulse on a multilayer coupled microstrip for different spacings ($l = 100$ mm, $\tau = 50$ ps, $A = 5$, $w = 1.5$ mm $h_{U1} = \infty$, $h_{U2} = 0.15$ mm, $h_{L3} = 0.2$ mm, $h_{L2} = 1.3$ mm, $h_{L1} = 0.5$ mm, $\epsilon_{rU1} = 1.0$, $\epsilon_{rU2} = 3.5$, $\epsilon_{rL3} = 5.5$, $\epsilon_{rL2} = 12.2$, $\epsilon_{rL1} = 9.7$). (a) Signal line response. (b) Sense line response.

The strip spacing, s, is an important parameter in coupled microstrip design. In order to reduce the effects of even/odd-mode distortion, the strip spacing is increased; however, to reduce circuit dimensions, the spacing should be as small as possible. It is important then to be able to choose an appropriate spacing which is as small as possible and yet does not have an unacceptable amount of even/odd-mode distortion. There are three main considerations in assessing the effect of even/odd-mode distortion on pulse dispersion:

a) the reduction of amplitude in the signal line pulse;
b) the amplitude of the unwanted response in the sense line;
c) the amount of pulse spread in time.

The acceptable values of these parameters are determined by the specific circuit in question and are dependent on the type of pulse and the line length, as well as the physical parameters of the structure.

A complex structure is used to illustrate both the use of the recursive Green's function formulation and the effect of strip spacing on pulse distortion. The structure is an open microstrip with three dielectric layers below the center conductor, one cover layer, and open air above it, with dimensions and parameters as given in Fig. 6. The signal line response, plotted in Fig. 6(a), shows that at a spacing of about 5 mm, the effects of even/odd-mode distortion become secondary to dispersion distortion. In Fig. 6(b), the response on the sense line is detailed. Note that the positive peak of the response reaches a maximum amplitude at $s = 2.5$ mm, reducing slightly for $s = 1.5$ mm. This is because the amplitudes of the positive and negative peaks tend to approach a value that is one half the single line response as the even and odd modes begin to separate, as shown in Fig 2.

In this structure, ϵ_{ro} is less than ϵ_{re} and so the leading response on the sense line is negative. For single-layer, open microstrip structures (Fig. 1, $N = 1$ and $M = 1$), the odd mode always has a lower ϵ_{reff}. For multiple-layer structures, however, it is possible for the even mode to have a lower ϵ_{reff}. An example of this kind of structure is an open microstrip with two dielectric layers below the center conductor interface (Fig. 1, $N = 2$ and $M = 1$), where ϵ_{rL1} is sufficiently less than ϵ_{rL2}. Fig. 7(a) shows how the ϵ_{re} and ϵ_{ro}, as well as the ϵ_{reff} of a single isolated microstrip, vary as a function of the heights of the two substrates for a given total substrate height, operating frequency, and parameters as shown in Fig. 7. When the height ratio, h_1/h_{total}, is equal to either 0 or 1 (only ϵ_{rL2} or ϵ_{rL1} below), ϵ_{ro} is lower than ϵ_{re}, which is expected since these configurations are simply a single-layer microstrip. However, when the height ratio is between about 0.3 and 0.85, ϵ_{re} is lower than ϵ_{ro}. At two different height ratios ϵ_{re} is equal to ϵ_{ro}; therefore there is no even/odd-mode distortion at this frequency for those two configurations.

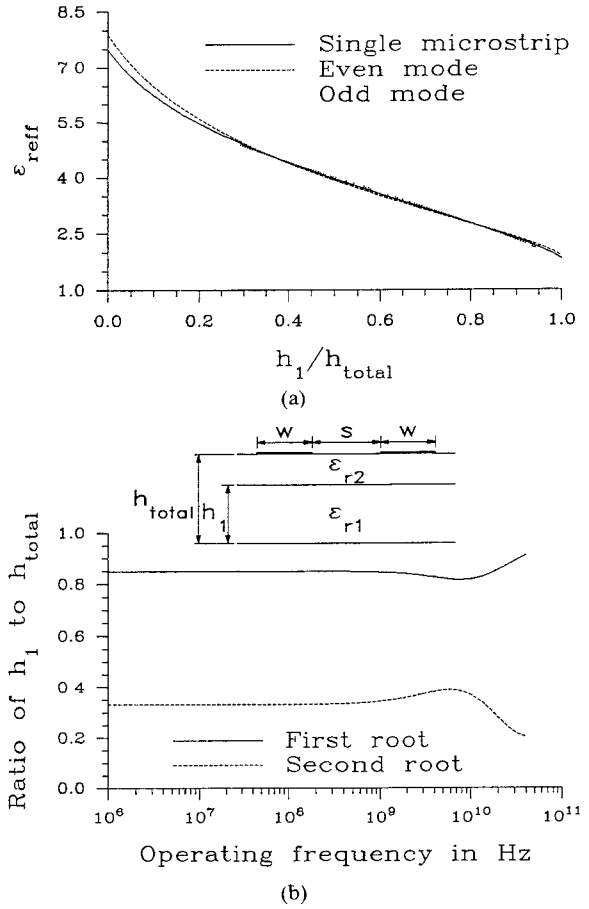

Fig. 7. Even/odd-mode behavior for two-layer open microstrip ($h_{total} = w = 1.5$ mm, $s = 3.0$ mm, $\epsilon_{rL2} = 9.7$, $\epsilon_{rL1} = 2.2$). (a) Effective dielectric constants versus height ratio of dielectric substrates, $f = 10$ GHz. (b) Location of zero even/odd-mode distortion points versus frequency.

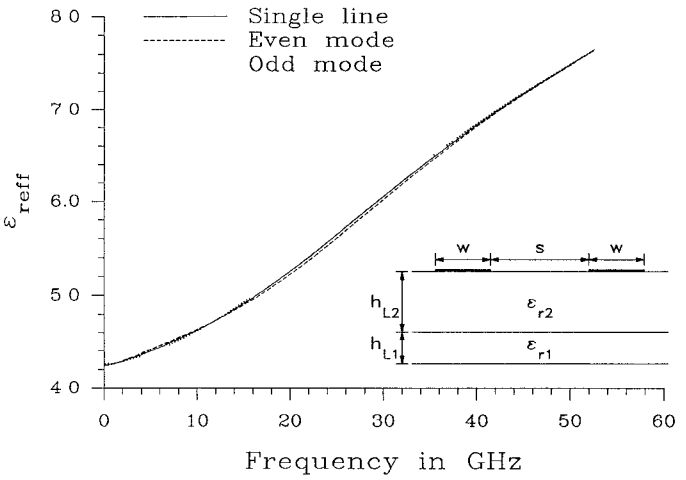

Fig. 8. Effective dielectric constants for coupled and single isolated microstrips on a low-distortion structure ($w = 1.5$ mm, $s = 3.0$ mm, $h_{L2} = 0.97$ mm, $h_{L1} = 0.53$ mm, $\epsilon_{r2} = 9.7$, $\epsilon_{r1} = 2.2$).

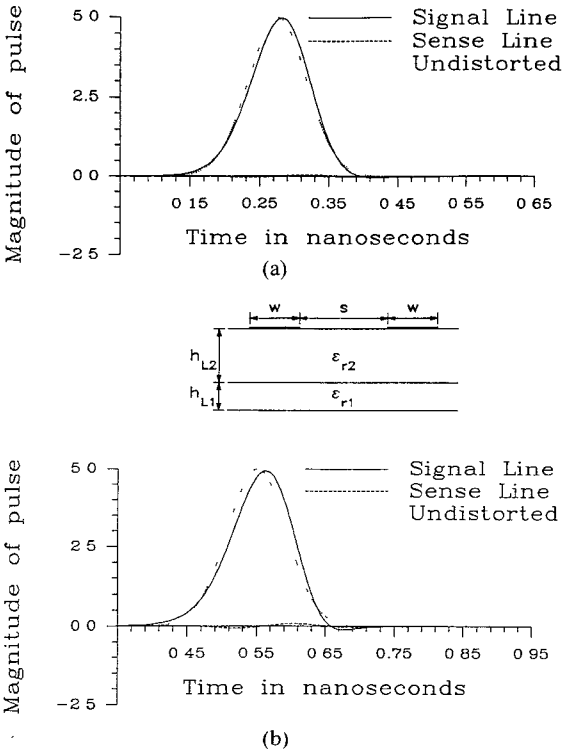

Fig. 9. Gaussian pulse distortion on a coupled microstrip for (a) $l = 40$ mm and (b) $l = 80$ mm ($\tau = 50$ ps, $A = 5$, $w = 1.5$ mm, $s = 3.0$ mm, $h_{L2} = 0.97$ mm, $h_{L1} = 0.53$ mm, $\epsilon_{r2} = 9.7$, $\epsilon_{r1} = 2.2$).

These zero dispersion points can be used to specify structural parameters where the lines are completely uncoupled, despite their close spatial proximity. The locations of the zero dispersion points, or roots, are plotted as a function of frequency in Fig. 7(b) for the structure shown. The total substrate height and dielectric constant of the top layer are the same as the structure used for Figs. 3–5. At frequencies higher than those shown in Fig. 7(b), the roots are not included because ϵ_{re} and ϵ_{ro} are approximately the same for all height ratios, making all of them zero dispersion points.

Since the structure in Figs. 3–5 is limited by its even/odd-mode distortion, it is advantageous to see if it is possible to remove this distortion by adding a second dielectric layer of appropriate height below. The original total substrate height is retained, as well as the upper substrate ($\epsilon_{rL2} = 9.7$); however a lower substrate with $\epsilon_{rL1} = 2.2$ is introduced. Since the Gaussian pulse used in the first case is of such short duration, its frequency spectrum contains significant components at frequencies where the zero distortion roots are varying widely. Thus it is not possible to obtain a configuration where there is no even/odd distortion for all the frequencies of interest. However, since the spectrum of the pulse falls off quadratically and since ϵ_{re} and ϵ_{ro} approach the same values at higher frequencies, it is more important to match the zero dispersion points for the lower part of the frequency spectrum. Thus a height ratio of 0.35 is chosen and the frequency characteristics of the three effective dielectric constants are plotted in Fig. 8.

While ϵ_{re} and ϵ_{ro} are not exactly equal for all frequencies, at lower frequencies (< 20 GHz) they differ by less than 0.9 percent. In addition, at two frequencies, 1.5 GHz and 11 GHz, ϵ_{re} and ϵ_{ro} are equal. Note that the largest difference between ϵ_{re} and ϵ_{ro} for this structure does not occur at zero frequency, but instead happens at 23 GHz,

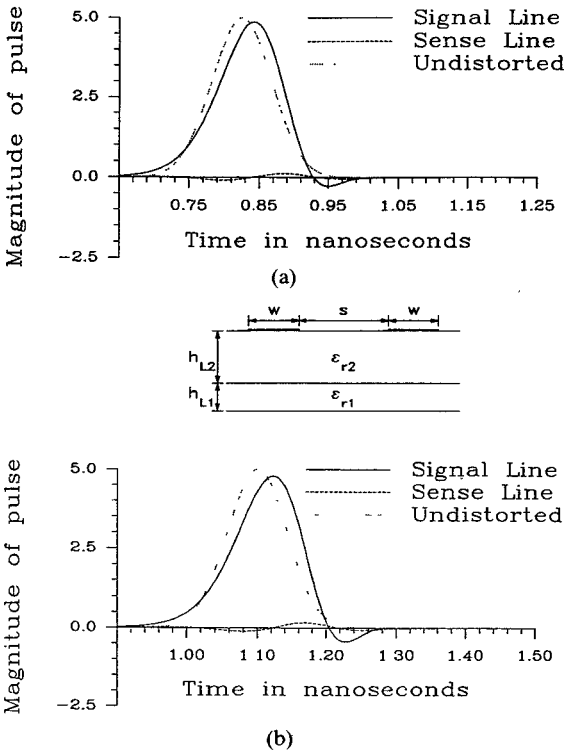

Fig. 10. Gaussian pulse distortion on a coupled microstrip for (a) $l = 120$ mm and (b) $l = 160$ mm ($\tau = 50$ ps, $A = 5$, $w = 1.5$ mm, $s = 3.0$ mm, $h_{L2} = 0.97$ mm, $h_{L1} = 0.53$ mm, $\epsilon_{r2} = 9.7$, $\epsilon_{r1} = 2.2$).

where they differ by 1.4 percent. At very high frequencies, the two ϵ_{reff}'s are almost equal, with less than a tenth of a percent difference.

Using these data for ϵ_{re} and ϵ_{ro}, the pulse responses for this structure, at the same distances used in Figs. 4 and 5, are shown in Figs. 9 and 10. The response for the single line is not shown, because there was no visible difference between it and the signal line response. In fact, at $l =$ 160 mm, the single and signal line pulses agree to better than 1 percent, showing that even/odd distortion has been almost completely eliminated. In addition, the response on the sense line has been reduced from 56 percent of the undistorted pulse in Fig. 5(b) to 3.2 percent in Fig. 10(b). An added benefit is that dispersion distortion has also been reduced. This is because lower dielectric constants produce less dispersion for the same substrate height.

VI. Conclusions

This paper used a variation of the spectral-domain technique to derive a recursive formulation of the Green's function that can handle any planar geometry. The mechanism of even/odd-mode distortion was discussed and results were presented showing how it compares to dispersion distortion in a simple structure. The pulse distortion for different strip spacings was shown for a very complex planar structure, illustrating the use of the recursive Green's function formulation as well as the constraint that even/odd-mode distortion places on choosing strip spacing. The effect of multiple dielectric layers on ϵ_{re} and ϵ_{ro} was discussed and it was shown that certain multilayer structures have no even/odd-mode distortion at certain frequencies. In particular, for a two-layer structure, this occurs for two different combinations of substrate heights when the bottom layer has a dielectric constant that is much lower than that of the top layer. This principle was applied in designing a coupled microstrip transmission line that had very low even/odd-mode distortion. It was shown that this structure had almost completely eliminated even/odd-mode distortion in the design, despite the very close spatial proximity of the lines.

Acknowledgment

The authors would like to thank Dr. J. W. Mink of the Electronics Division, Army Research Office, for his interest and support of the project.

References

[1] K. K. Li., G. Arjavalingam, A. Dienes, and J. R. Whinnery, "Propagation of picosecond pulses on microwave striplines," *IEEE Trans. Microwave Theory Tech.*, vol. MTT-30, pp. 1270–1273, Aug. 1982.

[2] J. F. Whitaker, T. B. Norris, G. Mourou, and T. Y. Hsiang, "Pulse dispersion and shaping in microstrip lines," *IEEE Trans. Microwave Theory Tech.*, vol. MTT-35, pp. 41–47, Jan. 1987.

[3] R. L. Veghte and C. A. Balanis, "Dispersion of transient signals in microstrip transmission lines," *IEEE Trans. Microwave Theory Tech.*, vol. MTT-34, pp. 1427–1436, Dec. 1986.

[4] G. Hasnain, G. Arjavalingam, A. Dienes, and J. R. Whinnery, "Dispersion of picosecond pulses on microstrip transmission lines," *Picosec. Optoelectron.*, vol. 439, pp. 159–163, Aug. 1983.

[5] B. H. Kolner, D. M. Bloom, and P. S Cross, "Picosecond optical electronic measurements," *Picosec. Optoelectron.*, vol. 439, pp. 149–152, Aug. 1983.

[6] T. Leung and C. A. Balanis, "Attenuation distortion of transient signals in microstrip," *IEEE Trans. Microwave Theory Tech.*, vol. 36, pp. 765–769, Apr. 1988.

[7] T. Leung and C. A. Balanis, "Pulse dispersion distortion in open and shielded microstrips using the spectral-domain method," *IEEE Trans. Microwave Theory Tech.*, vol. 36, pp. 1223–1226, July 1988.

[8] C. K. Tzuang and T. Itoh, "High-speed pulse transmission along a slow-wave CPW for monolithic microwave integrated circuits," *IEEE Trans. Microwave Theory Tech.*, vol. MTT-35, pp. 697–704, Aug. 1987.

[9] G. Hasnain, A. Deines, and J. R. Whinnery, "Dispersion of picosecond pulses in coplanar transmission lines," *IEEE Trans. Microwave Theory Tech.*, vol. MTT-34, pp. 738–741, June 1986.

[10] J. F. Whitaker, R. Sobolewski, D. R. Dykaar, T. Y. Hsiang, and G. A. Mourou, "Propagation model for ultrafast signals on superconducting dispersive striplines," *IEEE Trans. Microwave Theory Tech.*, vol. 36, pp. 277–285, Feb. 1988.

[11] A. R. Djordjevic, T. K. Sarkar, and R. F. Harrington, "Time-domain response of multiconductor transmission lines," *Proc. IEEE*, vol. 75, pp. 743–764, June 1987.

[12] A. R. Djordjevic, T. K. Sarkar, and R. F. Harrington, "Analysis of lossy transmission lines with arbitrary terminal networks," *IEEE Trans. Microwave Theory Tech.*, vol. MTT-34, pp. 660–666, June 1986.

[13] J. P. Gilb, "Transient signal analysis of multilayer multiconductor microstrip transmission lines," M.S. thesis, Arizona State University, 1989.

[14] T. Itoh and R. Mittra, "Spectral-domain approach for calculating the dispersion characteristics of microstrip lines," *IEEE Trans. Microwave Theory Tech.*, vol. MTT-21, pp. 496–499, July 1973.

[15] M. Kobayashi and F. Ando, "Dispersion characteristics of open microstrip lines," *IEEE Trans. Microwave Theory Tech.*, vol. MTT-35, pp. 101–105, Feb. 1987.

[16] N. Das and D. Pozar, "A generalized spectral-domain Green's function for multilayer dielectric substrates with application to multilayer transmission lines," *IEEE Trans. Microwave Theory Tech.*, vol. MTT-35, pp. 326–335, Mar. 1987.

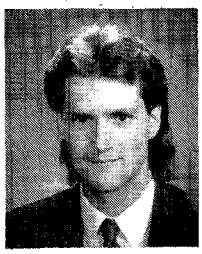

James P. Gilb (S'83) was born in Phoenix, AZ, on March 15, 1965. He received the bachelor of science degree in electrical engineering in 1987 and the master of science degree in electrical engineering in 1989, both from Arizona State University. He is currently pursuing the Ph.D. degree in electrical engineering there. His current interests are full-wave solutions of discontinuities and dielectric losses in planar waveguide structures.

Mr. Gilb is a member of Tau Beta Pi and Eta Kappa Nu.

✠

Constantine A. Balanis (S'62–M'68–SM'74–F'86) was born in October 1938, in Trikala, Greece. He received the B.S.E.E. degree from Virginia Polytechnic Institute, Blacksburg, in 1964, the M.E.E. degree from the University of Virginia, Charlottesville, in 1966, and the Ph.D. degree in electrical engineering from Ohio State University, Columbus, in 1969.

From 1964 to 1970 he was with NASA, Langley Research Center, Hampton, VA. In 1970 he joined the Department of Electrical Engineering, West Virginia University, Morgantown. He is now a Full Professor in the Department of Electrical and Computer Engineering and Director of the Telecommunications Research Center, Arizona State University, Tempe. He teaches graduate and undergraduate courses in electromagnetic theory, microwave circuits, and antennas. His research interests are in low- and high-frequency numerical antenna and scattering techniques, electromagnetic wave propagation in microwave integrated circuit transmission lines, and reconstruction (inversion) methods. He received for 1987–88 the Graduate Teaching Excellence Award, School of Engineering, Arizona State University.

Dr. Balanis is a member of ASEE, Sigma Xi, Tau Beta Pi, Eta Kappa Nu, and Phi Kappa Phi. He has served as Associate Editor of the IEEE TRANSACTIONS ON ANTENNAS AND PROPAGATION (1974–1977) and the IEEE TRANSACTIONS ON GEOSCIENCE AND REMOTE SENSING (1982–1984). He was editor of the *Newsletter* for the IEEE Geoscience and Remote Sensing Society (1982–1983) and Vice-President of the IEEE Geoscience and Remote Sensing Society (1984). He is author of *Antenna Theory: Analysis and Design* (John Wiley & Sons, New York, 1982) and *Advanced Engineering Electromagnetics* (John Wiley & Sons, New York, 1989).